AD_____

CONTRACT NUMBER DAMD17-94-C-4047

TITLE: Crystallographic Studies of the Anthrax Lethal Toxin

PRINCIPAL INVESTIGATOR: Christin A. Frederick, Ph.D.

CONTRACTING ORGANIZATION: Dana Farber Cancer Institute
Boston, Massachusetts 02115

REPORT DATE: January 1997

TYPE OF REPORT: Final

PREPARED FOR: Commander
U.S. Army Medical Research and Materiel Command
Fort Detrick, Frederick, Maryland 21702-5012

DISTRIBUTION STATEMENT: Approved for public release;
distribution unlimited

The views, opinions and/or findings contained in this report are those of the author(s) and should not be construed as an official Department of the Army position, policy or decision unless so designated by other documentation.

# REPORT DOCUMENTATION PAGE

*Form Approved*
*OMB No. 0704-0188*



| 1. AGENCY USE ONLY *(Leave blank)* | 2. REPORT DATE | 3. REPORT TYPE AND DATES COVERED |
|---|---|---|
| | January 1997 | Final (1 Jul 94 - 31 Dec 96) |

**4. TITLE AND SUBTITLE** Crystallographic Studies of the Anthrax Lethal Toxin

**5. FUNDING NUMBERS**
DAMD17-94-C-4047

**6. AUTHOR(S)**
Christin A. Frederick, Ph.D.

**7. PERFORMING ORGANIZATION NAME(S) AND ADDRESS(ES)**
Dana Farber Cancer Institute
Boston, Massachusetts 02115

**8. PERFORMING ORGANIZATION REPORT NUMBER**

**9. SPONSORING/MONITORING AGENCY NAME(S) AND ADDRESS(ES)**
U.S. Army Medical Research and Materiel Command
Fort Detrick
Frederick, Maryland 21702-5012

**10. SPONSORING/MONITORING AGENCY REPORT NUMBER**

**11. SUPPLEMENTARY NOTES**

**12a. DISTRIBUTION / AVAILABILITY STATEMENT**
Approved for public release; distribution unlimited

**12b. DISTRIBUTION CODE**

**13. ABSTRACT** *(Maximum 200*

Protective Antigen (PA) is the central component of the three-part protein toxin secreted by *Bacillus anthracis,* the organism responsible for anthrax. Following proteolytic activation on the host cell surface, PA forms a membrane-inserting heptamer that translocates the toxic enzymes into the cytosol. We have solved the crystal structure of monomeric PA at 2.1 Å resolution and the water-soluble heptamer at 4.5 Å resolution. The monomer is organized mainly into antiparallel b-sheets and has four domains: an N-terminal domain containing two calcium ions; a heptamerization domain containing a large flexible loop implicated in membrane insertion; a small domain of unknown function; and a C-terminal receptor-binding domain. Removal of a 20 kDa fragment from the N-terminal domain permits assembly of the heptamer, a ring-shaped structure with a negatively charged lumen, and exposes a large hydrophobic surface for binding the toxic enzymes. We present a model of pH-dependent membrane insertion involving formation of a porin-like membrane-spanning b barrel. These studies greatly enhance current understanding of the mechanism of anthrax intoxication, and will be useful in the design of recombinant anthrax vaccines.

| 14. SUBJECT TERMS | 15. NUMBER OF PAGES |
|---|---|
| Anthrax, Toxins, BD, BL2 | 29 |
| | 16. PRICE CODE |

| 17. SECURITY CLASSIFICATION OF REPORT | 18. SECURITY CLASSIFICATION OF THIS PAGE | 19. SECURITY CLASSIFICATION OF ABSTRACT | 20. LIMITATION OF ABSTRACT |
|---|---|---|---|
| Unclassified | Unclassified | Unclassified | Unlimited |

FOREWORD

Opinions, interpretations, conclusions and recommendations are those of the author and are not necessarily endorsed by the U.S. Army.

___ Where copyrighted material is quoted, permission has been obtained to use such material.

___ Where material from documents designated for limited distribution is quoted, permission has been obtained to use the material.

___ Citations of commercial organizations and trade names in this report do not constitute an official Department of Army endorsement or approval of the products or services of these organizations.

___ In conducting research using animals, the investigator(s) adhered to the "Guide for the Care and Use of Laboratory Animals," prepared by the Committee on Care and use of Laboratory Animals of the Institute of Laboratory Resources, National Research Council (NIH Publication No. 86-23, Revised 1985).

___ For the protection of human subjects, the investigator(s) adhered to policies of applicable Federal Law 45 CFR 46.

___ In conducting research utilizing recombinant DNA technology, the investigator(s) adhered to current guidelines promulgated by the National Institutes of Health.

___ In the conduct of research utilizing recombinant DNA, the investigator(s) adhered to the NIH Guidelines for Research Involving Recombinant DNA Molecules.

___ In the conduct of research involving hazardous organisms, the investigator(s) adhered to the CDC-NIH Guide for Biosafety in Microbiological and Biomedical Laboratories.

PI - Signature 1/29/97 Date

TABLE OF CONTENTS

REPORT DOCUMENTATION PAGE . . . . . 2
FOREWORD . . . . . 3
INTRODUCTION
1. Background . . . . . 5
2. Purpose and scope of research . . . . . 6
3. Outline of current report . . . . . 6
BODY
1. Structure determination of the PA monomer . . . . . 7
2. Structure determination of the $PA_{63}$ heptamer . . . . . 9
3. Description of the PA monomer . . . . . 10
a. Domain 1 . . . . . 11
b. Domain 2 . . . . . 11
c. Domain 3 . . . . . 11
d. Domain 4 . . . . . 12
4. Description of the $PA_{63}$ heptamer . . . . . 12
5. Insights into PA activity
a. Receptor binding . . . . . 12
b. Proteolytic activation . . . . . 12
c. Heptamer formation . . . . . 13
d. EF/LF binding . . . . . 13
e. Membrane insertion . . . . . 13
f. Translocation of EF/LF . . . . . 14
CONCLUSIONS . . . . . 15
FIGURES
1. Steps in anthrax intoxication of the host cell . . . . . 16
2. Ribbon diagram of PA . . . . . 17
3. Secondary structure assignment . . . . . 18
4. Domain 1 . . . . . 19
5. The calcium binding site . . . . . 20
6. Domain 2 . . . . . 21
7. Domain 3 . . . . . 22
8. Domain 4 . . . . . 23
9. Ribbon diagram of the $PA_{63}$ heptamer..... . . . . 24
10. A possible mechanism of membrane insertion . . . . . 25
REFERENCES . . . . . 26
BIBLIOGRAPHY . . . . . 29

## *INTRODUCTION*

### 1. Background

The study of anthrax has played an important role in the history of medicine, leading to the establishment of Koch's postulates (1) and to the development of the first bacterial vaccine (2,3). Outbreaks of anthrax continue to be reported, particularly in developing nations (4). Public awareness has been greatly raised by recent investigations into the Sverdlovsk outbreak of 1979 (5-7) and by the threat of anthrax spores being used as an agent of biological warfare (8).

Anthrax is caused by the spore-forming bacterium, *Bacillus anthracis,* and primarily afflicts herbivores such as cattle and sheep (9). Humans acquire the disease from infected animals or their products in one of three forms: a cutaneous form characterized by black pustules; a gastrointestinal form caused by eating contaminated meat; and a pulmonary form caused by inhaling anthrax spores, which is usually fatal within a few days of infection (10).

Two factors account for the virulence of *B. anthracis* : a poly-**D**-glutamic acid capsule that protects against bactericidal components of host sera (11), and "anthrax toxin". Anthrax toxin refers collectively to three secreted proteins: the edema factor (EF, 89 kDa), the lethal factor (LF, 90 kDa), and the protective antigen (PA, 83 kDa) (12). Although these proteins are individually non-toxic, PA combined with EF produces edema in the skin of guinea pigs and rabbits (13), while PA combined with LF lyses mouse macrophages (14) and induces death in experimental animals (15).

The action of anthrax toxin on the host cell has recently been reviewed (12), and is illustrated in figure 1. PA binds with high affinity ($K_d$ ~1 nM) to a protein receptor found on most mammalian cells (11, 16). Cleavage by a cell-surface protease, probably furin (17, 18), releases an N-terminal 20 kDa fragment, $PA_{20}$, and permits the 63 kDa fragment, $PA_{63}$, to form a heptamer (19) and to bind LF or EF with high affinity (11). The heptamer is water-soluble at neutral or basic pH and inserts into membranes at acidic pH, forming cation-selective channels in both artificial lipid bilayers (20) and cells (21). The complex of $PA_{63}$ with LF or EF then undergoes receptor-mediated endocytosis (22). Acidification of the endocytic vesicle leads to insertion of $PA_{63}$ into the endosomal membrane and translocation of EF or LF into the cytosol, where they exert toxic catalytic effects: calmodulin-dependent adenylate cyclase activity in the case of EF (23,24); and an unknown activity in the case of LF. In the "A-B" toxin nomenclature (25) PA is the B (binding) moiety, and LF and EF are alternative A (enzymatically active) moieties. Homologues of PA have been found in several spore-forming Gram-positive bacteria (e.g. the Iota-*b* toxin in *C. perfringens* (26) and the Vegetative Insecticidal Protein (VIP1) toxins in *B. cereus*

and *B. thuringiensis* (27) ) and share the ability to translocate toxic enzymes into the host cytosol.

PA is the most immunogenic of the three anthrax toxin proteins (28,29) and, as implied by its name, is the principal active component in anthrax vaccines (30). In the United States, the currently licensed human vaccine, MDPH-PA, is obtained from a non-virulent strain of *B. anthracis* and consists of aluminum hydroxide-adsorbed supernatant material, which is primarily PA (31). Immunization with MDPH-PA requires multiple doses, produces undesired side-effects in some individuals, and has diminished efficacy against certain virulent strains of *B. anthracis* (31-33). There is therefore an obvious need to improve the efficacy of the human vaccine.

## 2. Purpose and scope of research

The work described here aims at determining the atomic resolution structure of the anthrax protective antigen in its monomeric and oligomeric forms. These structures should lead to a greater understanding of anthrax intoxication by providing insight into the receptor binding, EF/LF binding, oligomerization, membrane channel formation, and EF/LF translocation activities of PA. This information should aid in the development of an improved vaccine by facilitating the construction of recombinant proteins that are deficient in key activities but retain high immunogenicity. It should also benefit new biomedical applications, such as the use of anthrax toxin as a "targeted toxin" (34).

## 3. Outline of current report

This report summarizes research carried out from July 1, 1994 to December 31, 1996. During this period we solved the crystal structure of monomeric PA at 2.1 Å resolution and the structure of the water-soluble $PA_{63}$ heptamer at 4.5 Å resolution. Here we describe these structures and the insights they provide into the mechanism of anthrax intoxication. Much of the material in this report appears in earlier quarterly and annual reports. The key results of our work have recently been published (35).

*BODY*

**1. Structure determination of the PA monomer**

Two crystal forms were used in the structure determination. Crystal form 1 grows from 14-18% PEG 1000, 10% glycerol and 50 mM HEPES pH 7.5 at 4° C and adopts space group $P2_12_12_1$ with $a$=119.8 Å, $b$=73.8 Å, $c$=95.0 Å. Crystal form 2 grows from 12-18% PEG 8K and 50 mM citrate pH 6.0 at 4°C, and adopts space group $P2_12_12_1$ with $a$=99.3 Å, $b$=93.7 Å, $c$=82.0 Å. Crystallographic statistics are summarized in table 1. All data sets listed in table 1 are from crystal form 1 except Nat2. Three native data sets were used: Nat1a for the MIR phasing, and Nat1b and Nat2 for refinement. Nat1b was collected at 4° C at SSRL beam line 7-1 ($\lambda$=1.08 Å) on a MAR image plate, while Nat2 was collected at -170°C using 30% PEG 200 as the cryoprotectant on a CCD area detector at CHESS beam line A-1 ($\lambda$=0.92 Å). Nat1b and Nat2 were processed with DENZO and SCALEPACK(36). All other data sets were collected at 4° C on a Xuong-Hamlin Multiwire area detector using Cu K$\alpha$ radiation, and were processed with UCSD software (37).

Crystal form 1 was solved by multiple isomorphous replacement (MIR). Soaking conditions for heavy metal derivatives were as follows: MMN1 and MMN2, methylmercuric nitrate at 1 mM for 5h and 10 mM for 1h, respectively; MA, 10 weeks in 10 mM mersalyl acid; $K_2PtCl_4$, 3 days at 10 mM; $K_2PtBr_6$, 3 days at 2 mM and 3 days at 4 mM; TTP, 2 days in 5 mM dipotassium tetrakis(thiocyanato)platinate (II); $UO_2(NO_3)_2$, 0.1 to 1 mM over 4 days; $KI_3$, 6 days in 10 mM iodine and 10 mM potassium iodide. Heavy atom positions were determined by Patterson and cross-Fourier methods, and atomic parameters were refined using MLPHARE (38). An MIR map calculated at 3.5 Å showed a clear solvent boundary and several elements of secondary structure. An initial model consisting of ~300 glycine and alanine residues was built using FRODO (39) and refined at 2.5 Å resolution with XPLOR (40). Recombining model phases with the experimental phases led to an improved map and allowed additional residues to be modelled. The initial sequence assignment was facilitated by iodinating crystals to specifically label tyrosines and by mercurating crystals of two point mutants, Thr357→Cys and Ser623→Cys. Iterative cycles of phase recombination, manual model building and XPLOR refinement led to a nearly complete model, but several ambiguities persisted. These were resolved using crystal form 2, whose structure was solved by molecular replacement and refined at 2.1 Å resolution. Two strong peaks of density in an $F_o$-$F_c$ map were identified as calcium ions on the basis of coordination geometry, bond distances, and the prevalence of acidic ligands. The presence of calcium was confirmed by atomic absorption spectroscopy (T. Koehler and R.J. Collier, unpublished).

**TABLE 1.** Crystallographic statistics.

1. Monomeric PA.

| Data Set | Nat1a | Nat1b | Nat2 | MMN1† | MMN2 | MA | $K_2PtCl_4$ | $K_2PtBr_6$ | TTP | U | $KI_3$ |
|---|---|---|---|---|---|---|---|---|---|---|---|
| Resolution (Å) | 3.2 | 2.5 | 2.1 | 3.2 | 3.2 | 4.0 | 3.6 | 3.2 | 3.6 | 4.0 | 3.4 |
| Unique | 13012 | 28421 | 45183 | 11423 | 13129 | 6686 | 9359 | 12073 | 8180 | 7112 | 10093 |
| Completeness (%) | 90 | 96 | 91 | 85 | 90 | 92 | 96 | 83 | 82 | 94 | 89 |
| Redundancy | 7.0 | 3.3 | 3.0 | 4.2 | 3.8 | 2.9 | 2.4 | 2.6 | 3.3 | 4.0 | 4.3 |
| $R_{sym}$ (%) * | 4.1 | 6.6 | 6.7 | 4.7 | 9.9 | 4.5 | 4.0 | 7.0 | 5.1 | 7.0 | 7.1 |
| <I>/<σI> in outer shell | 4.8 | 10.7 | 4.0 | 3.4 | 1.5 | 8.2 | 6.6 | 4.8 | 4.2 | 3.8 | 3.5 |
| No. Sites | | | | 5 | 6 | 5 | 2 | 3 | 2 | 4 | 11 |
| $R_{iso}$ † | | | | 8.9 | 22.3 | 13.0 | 11.3 | 13.9 | 12.5 | 11.0 | 13.1 |
| $R_{Cullis}$ ‡ | | | | 0.72 | 0.71 | 0.86 | 0.90 | 0.80 | 0.81 | 0.89 | 0.88 |
| Phasing Power | | | | 1.1 | 1.2 | 0.7 | 0.6 | 0.9 | 0.6 | 0.5 | 0.6 |
| Mean overall figure of merit (20-3.2 Å) | | | | 0.58 | | | | | | | |

| Refinement statistics: | Resolution (Å) | R factor (%) ¶ | R (free) (%) # | rms bond lengths (Å)‖ | rms bond angles ‖ |
|---|---|---|---|---|---|
| crystal form 1 | 6-2.5 | 27.1 | 32.0 | 0.009 | 2.0° |
| crystal form 2 | 6-2.1 | 22.9 | 28.1 | 0.006 | 1.5° |

2. Heptameric $PA_{63}$

| Resolution Shell (Å) | 9.63 | 7.64 | 6.67 | 6.06 | 5.63 | 5.30 | 5.03 | 4.81 | 4.63 | 4.47 | Overall |
|---|---|---|---|---|---|---|---|---|---|---|---|
| Unique | 3876 | 3924 | 3893 | 3899 | 3856 | 3882 | 3897 | 3894 | 3869 | 2969 | 37959 |
| Completeness (%) | 96.5 | 99.2 | 99.4 | 99.4 | 99.5 | 99.4 | 99.7 | 99.6 | 99.6 | 76.6 | 99.1 |
| Redundancy | 2.7 | 2.8 | 2.8 | 2.8 | 2.8 | 2.8 | 2.8 | 2.8 | 2.8 | 2.1 | 2.8 |
| <I>/<σI> | 20.6 | 16.2 | 9.9 | 7.4 | 5.8 | 5.1 | 4.4 | 4.2 | 3.9 | 2.6 | 9.8 |
| $R_{sym}$ (%) * | 3.3 | 5.0 | 10.2 | 14.6 | 18.9 | 22.9 | 26.3 | 27.7 | 29.7 | 32.1 | 10.2 |
| Statistics of non-crystallographic symmetry phase refinement: | | | | | | | | | | | |
| Averaging R§ | 19.0 | 17.7 | 20.4 | 24.0 | 26.6 | 29.6 | 31.1 | 33.5 | 38.0 | 49.9 | 23.9 |
| Correlation** | 0.91 | 0.91 | 0.90 | 0.85 | 0.83 | 0.78 | 0.74 | 0.71 | 0.67 | 0.55 | 0.87 |

†Abbreviations for heavy metal derivatives are defined in the text.

*$R_{sym} = \Sigma\Sigma_i |\langle I\rangle - I_j| / \Sigma \langle I\rangle$. †$R_{iso} = \Sigma | F_{ph} - F_p | / \Sigma |F_p|$.

‡$R_{Cullis} = \Sigma | |F_{ph} \pm F_p| - F_{hc}| / \Sigma |F_{ph} \pm F_p|$ for centric reflections.

¶ R factor = $\Sigma | F_p - F_{p(calc)}| / \Sigma F_p$ for reflections with $F_p > 2\,\sigma(F_p)$

#$R_{free}$ is computed on a randomly selected 10% of the data which were excluded from refinement.

‖ The rms deviations from ideal values.

§ Averaging R = $\Sigma |F_O - F_C| / \Sigma |F_O|$

**Correlation coefficient = $\Sigma_h (\langle F_O\rangle - |F_{Oh}|)(\langle F_C\rangle - |F_{Ch}|) / \{\Sigma_h (\langle F_O\rangle - |F_{Oh}|)^2 - (\langle F_C\rangle - |F_{Ch}|)^2\}^{1/2}$

The model for crystal form 2 consists of 660 (out of 735) residues, 310 water molecules and 2 calcium ions. The model for crystal form 1 contains 680 residues, 2 calcium ions and no water molecules, and will be further refined. No density is seen in either crystal form for residues 1-13, 162-176 and 304-319, consistent with the protease sensitivity of these regions (11). Minor differences exist between the two crystal forms: residues 342-355 are ordered in crystal form 1 (pH 7.5) and in the $PA_{63}$ heptamer (pH 8.5), but are disordered in crystal form 2 (pH 6.0). Residues 511-516 of domain 3 form helix $3\alpha_1$ in crystal form 1 and in the $PA_{63}$ heptamer, but are disordered in crystal form 2. In order to further investigate the order $\rightarrow$ disorder transition mentioned above we recently collected two additional data sets for crystal form 1 using synchrotron radiation. One data set was collected from crystals grown at pH 8.5 and the other was collected from crystals grown at pH 7.5 and then soaked for 2 hours at pH 4.5. Once processed, these two data sets should permit us to determine whether the conformational differences between crystal forms 1 and 2 are due to different crystal lattices or to the pH.

## 2. Structure determination of the $PA_{63}$ heptamer

Crystals of the heptamer grow at room temperature from 2-5% PEG 8K, 100 mM $CaCl_2$ and 50 mM TRIS pH 8.5, and belong to space group $P2_1$, with $a$=142.8Å, $b$=148.3Å, $c$=164.1Å and $\beta$ = 107.9°. Data were collected at -170°C using 30% ethylene glycol as a cryoprotectant on a MAR image plate at ESRF beam line BM14 ($\lambda$=0.945 Å). A self-rotation function revealed a peak on the $\kappa$=51° section that was 68% as high as the origin peak, indicating the presence of one heptamer per asymmetric unit, with the 7-fold axis parallel to the crystallographic 2-fold screw along $b$. A cross rotation function calculated using domains 1' to 4 of the monomer structure gave an unambiguous solution at 8.5 $\sigma$ above the mean, and other strong peaks related by non-crystallographic symmetry. A translation search for one monomer gave a clear peak at 9.9 $\sigma$ above the mean, with the next noise peak at 2.9 $\sigma$. Clear solutions were also obtained for the other monomers, which when placed relative to the same origin by a combined translation function gave a center of mass in good agreement with the position deduced from the native Patterson. The heptamer model showed good packing in the crystal and was consistent with electron micrographs. Rigid body refinement of the 7 monomers caused a drop in the crystallographic R-factor from 0.48 to 0.41, and a similar drop in $R_{free}$, calculated using thin shells of reflections comprising 5% of unique measurements. An additional drop in $R_{free}$ was obtained by refining the four domains of each monomer as independent rigid bodies. The resulting coordinates were used to define the non-crystallographic symmetry operators. Cycles of 7-fold averaging were performed with RAVE (41), starting from a set of random phases and a mask covering one of the monomers. The averaging R-factor converged

to 23.9% for all measurements from 40-4.5 Å, and the real-space correlation coefficients relating the monomers were all 0.90 or higher. The rigid-body refined model showed good fit to the averaged map, which showed well-resolved backbone density but little density for side chains. The strongest features in the map were at 6 σ above the mean, and corresponded to the calcium ion sites. Minor conformational changes were readily apparent, including shifts in individual helices in domains 1' and 3 and a shift in the hairpin formed by residues 194-204. The model was adjusted in these regions and further rigid body refinement led to a crystallographic R factor of 32% and a $R_{free}$ of 36%. The model has not been further refined for lack of high resolution data.

### 3. Description of the PA Monomer.

Protective Antigen is a tall slender molecule with dimensions 100 Å x ~50 Å x 30 Å. A ribbon diagram of PA is shown in figure 2. The monomer is organized mainly into antiparallel β-sheets and has four domains: an N-terminal domain (Domain 1) containing two calcium ions and the furin cleavage site; a heptamerization domain (Domain 2) containing a large flexible loop implicated in membrane insertion; a small domain of unknown function (Domain 3); and a C-terminal receptor-binding domain (Domain 4).The domain assignments are summarized in table 2.

**Table 2.** Domains of PA

| Domain | | Residues | Activity | Furin fragment |
|---|---|---|---|---|
| 1 | ($PA_{20}$) | 1-167 | blocks oligomerization and EF/LF binding | $PA_{20}$ |
| | (1') | 168-258 | $Ca^{2+}$ binding EF/LF binding? | |
| 2 | | 259-487 | oligomerization membrane insertion | $PA_{63}$ |
| 3 | | 488-595 | unknown | |
| 4 | | 596-735 | receptor binding | |

Domains 1 and 2 are roughly equal in size and twice as large as domains 3 and 4. The cleavage by furin which results in the $PA_{20}$ and $PA_{63}$ fragments does not occur

between domains, but within domain 1. Domains 1, 2 and 3 are intimately associated, but domain 4 has limited contact with the adjacent domains. High sequence similarity over the first 600 residues and strictly conserved calcium-binding motifs indicate that the homologues share the same folds for domains 1, 2 and 3. The secondary structure and sequence similarity is illustrated in figure 3.

**a. Domain 1.** Domain 1 (residues 1 to 258) contains a large β sheet made of nine strands and a smaller sheet of five strands (Fig. 4). Proteolytic activation by the cell surface protease, furin, occurs at the sequence RKKR$^{167}$ in an exposed loop within domain 1, releasing an N-terminal 20 kDa fragment, $PA_{20}$ (residues 1-167), which plays no further role in intoxication. $PA_{20}$ forms an integral part of domain 1, and dissociation requires the rupture of a β sheet and exposure of a large hydrophobic surface, explaining why PA can be 'nicked' in vitro at the furin site without dissociating into two fragments (11). The remainder of domain 1, which we call domain 1' (residues 168-258), forms the N-terminus of the active 63 kDa fragment, $PA_{63}$. Domain 1' contains two calcium ions 4.3 Å apart, octahedrally coordinated by residues 177-188 and 222-235 in a variant of the EF-hand motif. Of the twelve calcium ligands, eight are carboxylate oxygens of acidic residues, three are main chain carbonyl oxygens and one is a water molecule (Fig. 5). The ions are almost completely buried and play a clear role in stabilizing the local three-dimensional structure.

**b. Domain 2.** Domain 2 (residues 259 to 487) is the longest domain (~65 Å) and is dominated by a β barrel with modified Greek key topology (Fig. 6). The barrel has elaborate excursions, including a large, chymotrypsin-sensitive loop implicated in membrane insertion. At the bottom of domain 2 is a stretch of residues (342-355) which are ordered in crystal form 1 (grown at pH 7.5) , but are disordered in crystal form 2 (grown at pH 6.0), exposing three hydrophobic residues to the solvent. This conformational change provides insight into the mechanism of membrane insertion (described below).

**c. Domain 3.** Domain 3 (residues 488 to 595) is the smallest of the domains and contains a four-stranded mixed β sheet, a hairpin, and four helices (Fig.7). This domain adopts the same fold as ferredoxins and domain A of toxic shock syndrome toxin-1. One of the helices protrudes significantly from the body of the molecule (Fig. 7, top). This helix is part of a stretch of residues (511-517) that are ordered in crystal form 1 but form a disordered loop in crystal form 2. The significance of this conformational change is not known. Domain 3 also contains five hydrophobic residues forming a flat, solvent exposed hydrophobic patch. In crystals of PA this patch is occupied by a

phenylalanine from another PA molecule. There is some evidence to suggest that domain 3 interacts with EF and LF (see below).

**d. Domain 4.** Domain 4 (residues 596 to 735) has an initial hairpin and helix, followed by a β-sandwich with an immunoglobulin-like fold. There is also a large loop (residues 703-720) which forms part of the interface between domains 2 and 4 and which is probably important for receptor binding activity (see below).

## 4. Description of the $PA_{63}$ heptamer

The water-soluble heptamer has a ring-like structure, 160 Å in diameter and 85 Å high (Fig.3), in agreement with electron micrographs. The central lumen has an average diameter of ~35Å, narrowing to ~20 Å in some places; it is polar and negatively charged (Fig. 3*d*), consistent with the cation-selectivity of $PA_{63}$ channels, but also includes a conserved phenylalanine (F427) in a solvent-exposed loop. Monomers pack like pie wedges, with domains 1' and 2 on the inside of the ring and domains 3 and 4 on the outside. Heptamer formation entails no major conformational changes in the monomers, and buries an extensive surface (2200 $Å^2$ per monomer) composed primarily of charged or polar residues from domain 2 and domain 1'. The tertiary structure of domain 1' remains largely unchanged upon heptamer formation, in spite of its torn β-sheet. The only significant movement occurs in the $1\beta_{12}$-$1\beta_{13}$ hairpin, which tilts upwards (by 5Å at its tip) in order to avoid steric clashes with its neighbour.

## 5. Insights into PA activity.

**a. Receptor binding.** Studies with blocking antibodies (42), proteolytic fragments (43) and deletion mutants (44) implicate domain 4 in host cell binding. Within the Ig-like fold of this domain, a 19-residue, highly accessible loop (between strands $4\beta_9$ and $4\beta_{10}$) is analogous to the antigen-binding CDR3 loop of antibodies and the receptor-binding loop of diphtheria toxin (45). The loop is a good candidate for mediating the PA-receptor interaction, since short C-terminal deletions which compromise the integrity of this loop eliminate cell binding (Fig. 8). The low degree of sequence homology shared by PA, iota-*b* and VIP1 in domain 4 suggests the three proteins bind to different host cell receptors.

### b. Proteolytic Activation

Proteolytic cleavage by furin does not occur between domains but within domain 1. Comparison of the monomer and heptamer structures show that no significant conformational changes occur upon proteolytic cleavage. Removal of $PA_{20}$ exposes a large surface almost exclusively on domain 1'. Domain 1' does not change conformation because it is stabilized by an extensive interface with domain 2 and internally by the two

calcium ions, which link the new N-terminus to residues in the core of domain 1' and prevent its becoming disordered.

### c. Heptamer formation

Although the removal of $PA_{20}$ is a prerequisite for heptamer formation, $PA_{20}$ does not mask the heptamerization interface; i.e., the molecular surface which becomes buried upon oligomerization is fully accessible in the monomeric PA structure. Substituting full-length PA for $PA_{63}$ in the heptamer results in a severe overlap among the seven $PA_{20}$ moieties, indicating that heptamerization prior to furin cleavage is blocked sterically by $PA_{20}$. Residues in the interface are highly conserved, suggesting that the homologous toxins also oligomerize.

### d. EF/LF binding

The removal of $PA_{20}$ completely exposes a large previously inaccessible surface on domain 1', creating a large flat hydrophobic patch on the "top" of the heptamer. This surface provides an obvious site for binding EF and LF, which bind $PA_{63}$ with high affinity (12, 46) but cannot bind full-length PA. This agrees with the finding that antibodies recognizing an epitope between residues 168 and 314 inhibit the binding of EF/LF (42). Other antibodies which inhibit EF/LF binding recognize an epitope between residues 581 and 601, suggesting that domain 3, which is adjacent to domain 1' (Fig. 2), may also interact with EF/LF.

### e. Membrane insertion

Since LF binds cells pre-incubated with $PA_{63}$ and blocks the ion conductance of pre-formed $PA_{63}$ membrane channels (46), the membrane-bound heptamer is likely oriented with domain 1' exposed to the extracellular environment, available to bind EF and LF, and with domain 4 and the bottom of domain 2 next to the membrane. How does the heptamer insert into membranes? Our heptamer structure lacks an obvious belt of hydrophobic residues, but proteolysis and mutagenesis experiments have implicated the large chymotrypsin-sensitive loop (residues 302-325) of domain 2 in the intoxication process (43, 47); and recent electrophysiological measurements on the membrane-inserted heptamer involving point mutations in this loop place residues 304, 306 and 308 inside the channel lumen (E.L. Benson, P.D. Huynh, A. Finkelstein, & R.J.Collier, unpublished data). The loop shows a conserved pattern of alternating hydrophilic and hydrophobic residues similar to that seen in porins (Fig. 10) and in the membrane-spanning hairpin of α-haemolysin (αHL) from *S. aureus* (48). In αHL, each monomer contributes an amphipathic hairpin to a 14-stranded β-barrel, and we propose that PA inserts into membranes in an analogous fashion. The diameter of $PA_{63}$ membrane channels determined by solute exclusion (~12Å) (49) is consistent with the size of such a barrel .

The loops project outwards from the side of the water-soluble heptamer. Their assembly into a β-barrel on the heptamer axis could be accomplished most simply if the Greek key motif formed by the first four strands of domain 2 ($2\beta_1$ to $2\beta_4$) were to unfold, with strands $2\beta_2$ and $2\beta_3$ peeling away from the edge of the domain (Fig 4 and 2c). This would involve breaking about as many hydrogen-bonds as are created on barrel formation, and is analogous to the conformational change proposed for the pH-induced conversion of transthyretin from its native to its amyloidogenic form (50). In vivo, the trigger for membrane-insertion is provided by acidification of the endosome. In vitro, channel formation by $PA_{63}$ in planar lipid bilayers is rapidly accelerated when the pH is lowered from 7.4 to 6.5 (20, 51), implicating the titration of histidines. Of the nine histidine residues in $PA_{63}$, five are contained within the Greek key motif of domain 2 (Fig. 2c, 4b). Two histidines (H304 and H310) lie within the $2\beta_2$-$2\beta_3$ loop. Two others (H263 and H299) form part of an unusual cluster of buried polar residues (including three arginines (R297, R490 and R504) and one glutamate (E502)) located at the top of the Greek key where the $2\beta_2$-$2\beta_3$ loop joins the body of domain 2. Local instability induced by protonation of these histidines would be relieved if strands $2\beta_2$ and $2\beta_3$ peeled away to expose the charged residues to solvent. The fifth histidine (H336) lies at the bottom of the Greek key in the loop connecting strands $2\beta_3$ and $2\beta_4$. Residues in this loop are ordered in crystals of PA grown at pH 7.5, but are disordered in the crystal form grown at pH 6.0, exposing three hydrophobic residues to solvent. This order → disorder transition may resemble the initial conformational changes that occur in the heptamer during membrane insertion.

**f. Translocation of EF/LF**

How $PA_{63}$ translocates EF and LF remains unknown. One possibility is that EF/LF cross the membrane by passing through the lumen of the $PA_{63}$ heptamer. The lumen of the heptamer is too small to permit passage of a native folded polypeptide but is sufficiently large to allow passage of α-helices and small subdomains. Thus, partial unfolding of EF and LF is required if translocation occurs by passage through the heptamer lumen. Some spectroscopic evidence suggests that EF and LF are capable of reversible unfolding at low pH. A role in translocation could conceivably be played by the two calcium ions buried in domain 1' (the putative EF/LF-binding domain): a lowered calcium concentration or a pH drop in the endosome might promote calcium release and modulate the $PA_{63}$:EF/LF interaction. $PA_{63}$ can translocate heterologous proteins fused to $LF_N$ (the highly charged N-terminal ~250 residues of LF responsible for binding to $PA_{63}$ (52)) into the cytosol. Recently, it has been shown that $PA_{63}$ can also translocate proteins fused to a polycationic peptide such as hexa- or octalysine(53). These polycationic leader peptides likely bind to the heptamer lumen, which is highly

negatively charged. Homology models built of VIP1 and Iota-*b* also have a negatively charged lumen, suggesting that this feature may be important for translocation, an acid-dependent process(14).

## *CONCLUSIONS*

We have realized our stated goals of solving the PA monomer and $PA_{63}$ heptamer structures. These structures have made a significant contribution to the anthrax field. Our finding that PA binds calcium ions raises the possibility that calcium plays an important role in PA activity. Also of interest is the finding that a large loop in domain 2 could feasibly form an amphipathic hairpin sufficiently long to span a lipid bilayer, suggesting that the membrane-inserted form of PA may resemble that of α-hemolysin. Our work suggests a number of approaches for designing an improved anthrax vaccine. For example, the channel forming properties of PA may be responsible for some of the negative side-effects observed with the current anthrax vaccine. The deletion of loop 2 should produce a PA molecule lacking channel-forming activity but maintaining a high degree of immunogenicity. Similarly, mutations in loop 4 may result in a molecule defective in heptamer formation, and hence in channel formation. Also, it should be possible to express the individual domains (the boundaries of which have been precisely defined by our crystallographic studies) as recombinant proteins and to test these for immunogenic and protective properties. Our data also suggest a range of mutations that can be used to test the functional role of other residues on the protein surface. Our collaborators are currently engaged in constructing such mutants.

The work described in this report has led to the following revised model of anthrax intoxication of the host cell: PA binds to cell receptors through domain 4, but is unable to oligomerize because of steric hindrance from domain 1. Cleavage at the furin site followed by dissociation of $PA_{20}$ results in heptamer formation, chiefly mediated by domain 2. LF or EF binds to the newly exposed domain 1', followed by receptor-mediated endocytosis of the complex. Acidification of the endocytic vesicle leads to a conformational change in the heptamer that permits seven flexible loops to insert into the membrane as a porin-like β barrel. This change likely involves the unfolding of a Greek key at the edge of domain 2. How EF and LF are translocated across the membrane remains a puzzle, but our heptamer structure suggests several testable hypotheses involving the anionic lumen of the heptamer pore and the calcium ions in domain 1'.

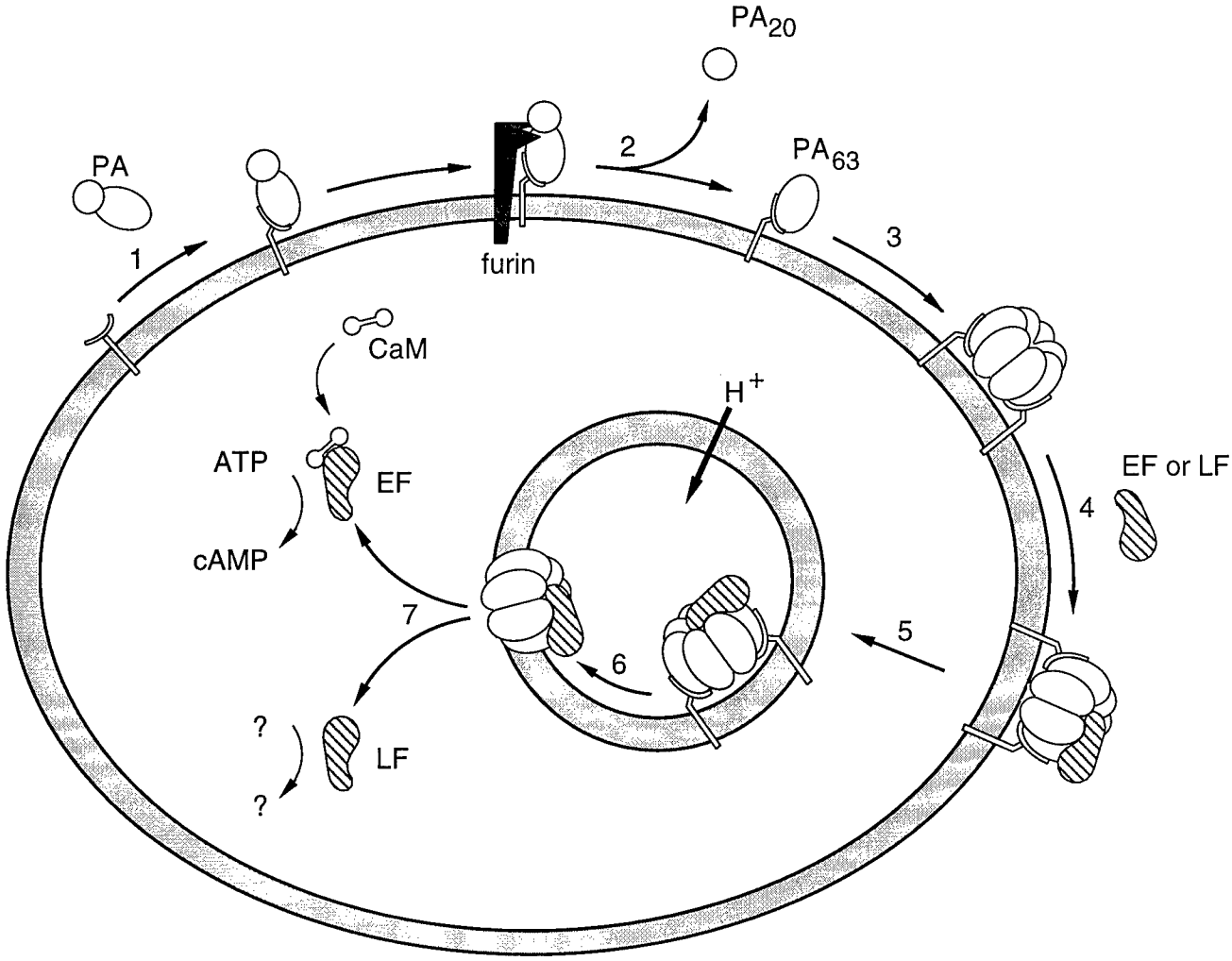


**Fig. 1.** Steps in anthrax intoxication of the host cell. The abbreviations are: PA, protective antigen; EF, edema factor; LF, lethal factor; CaM, calmodulin. *1.* PA binds to a host cell surface receptor. *2.* Furin or a furin–like cell surface protease cleaves PA, releasing the $PA_{20}$ fragment. *3.* $PA_{63}$ forms a heptamer. *4.* EF or LF binds to $PA_{63}$. *5.* Receptor–mediated endocytosis occurs. *6.* Acidification of the endocytic vesicle leads to membrane insertion of $PA_{63}$. *7.* Translocation of EF/LF into the cytosol, where they exert their toxic effects.

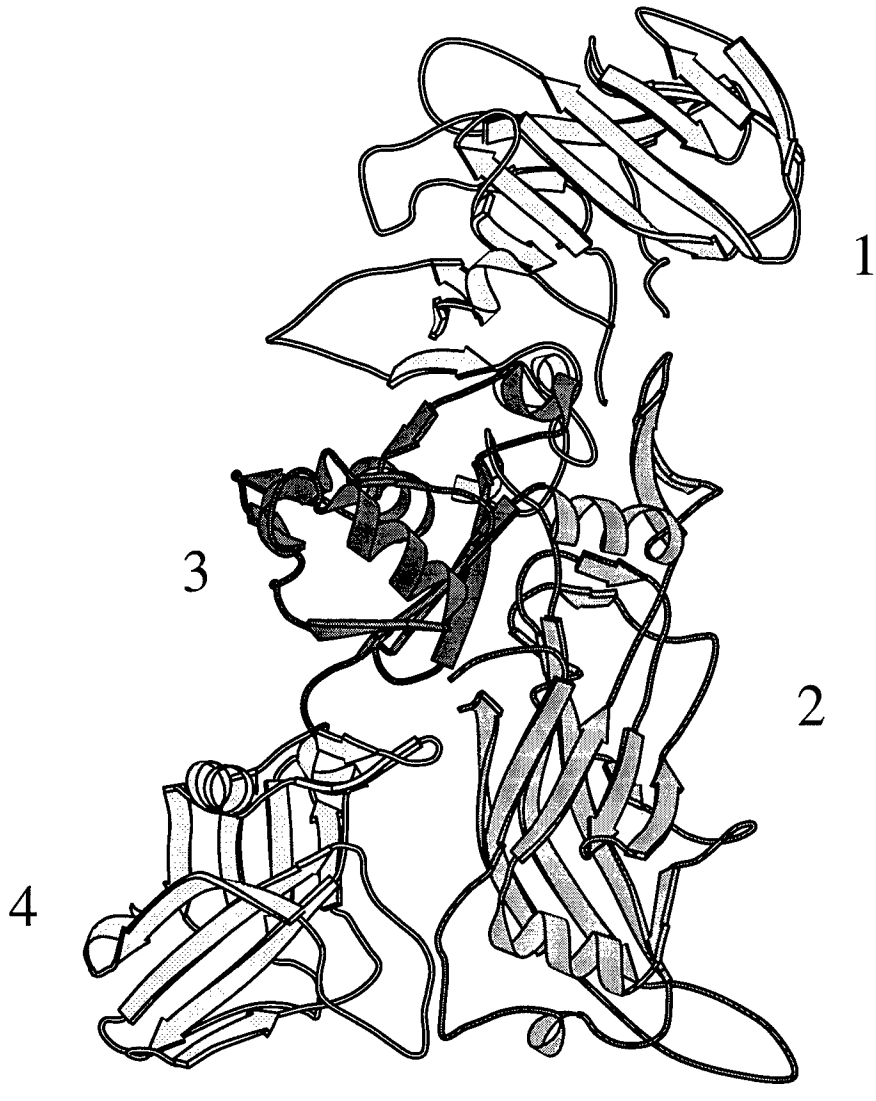


Fig.2. Ribbon diagram of PA.

The four domains are indicated.

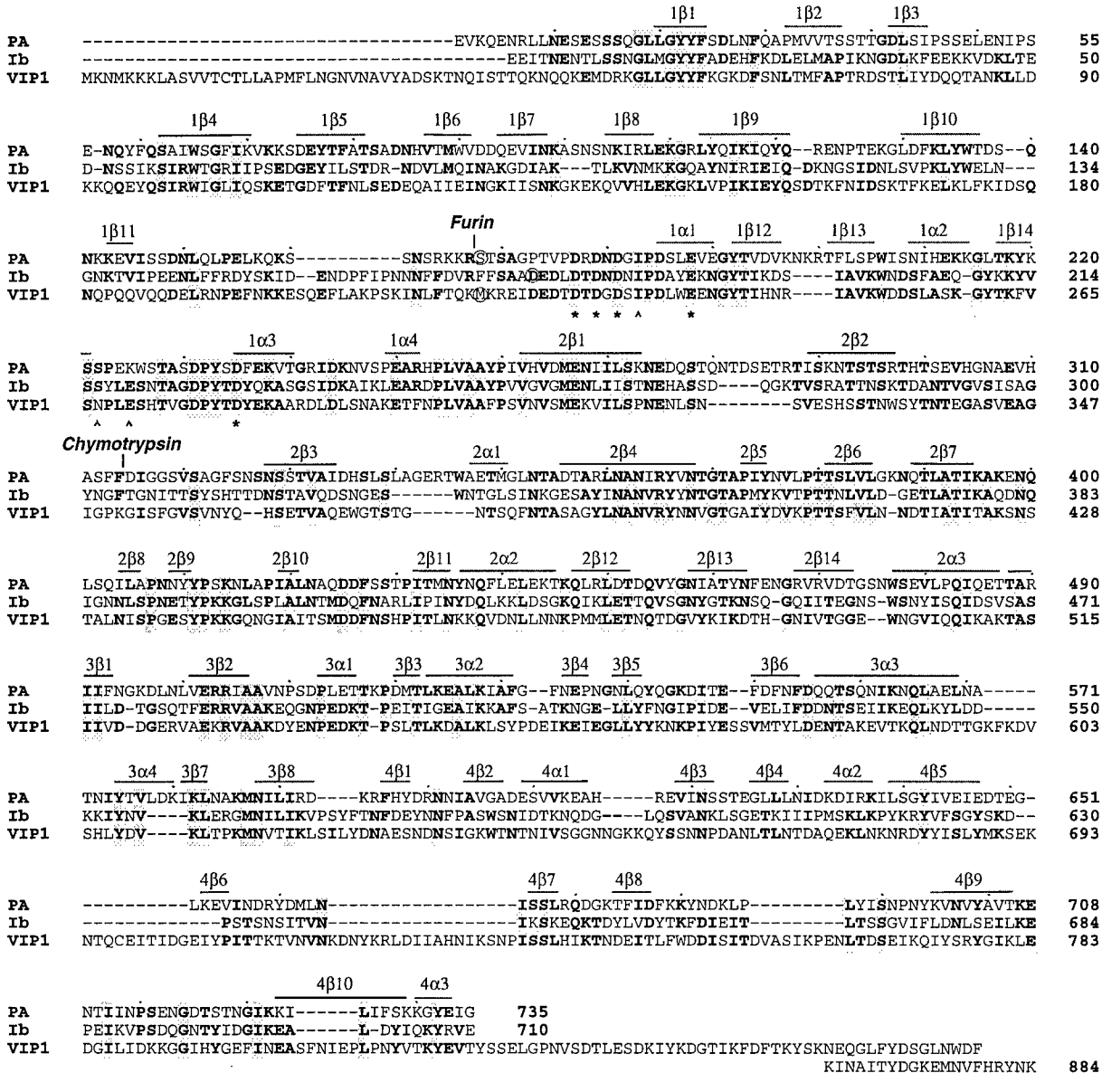


**Fig. 3.** Secondary structure assignment and alignment of the PA, Iota–*b* and VIP1 sequences. The numbering of each sequence is shown. Residues identical in two or more sequences are shown in bold, and those identical in all three are highlighted. The furin and chymotrypsin sites of PA are indicated Residues which ligate a calcium ion through a side chain or main chain oxygen atom are marked by an asterisk or a caret (^), respectively.

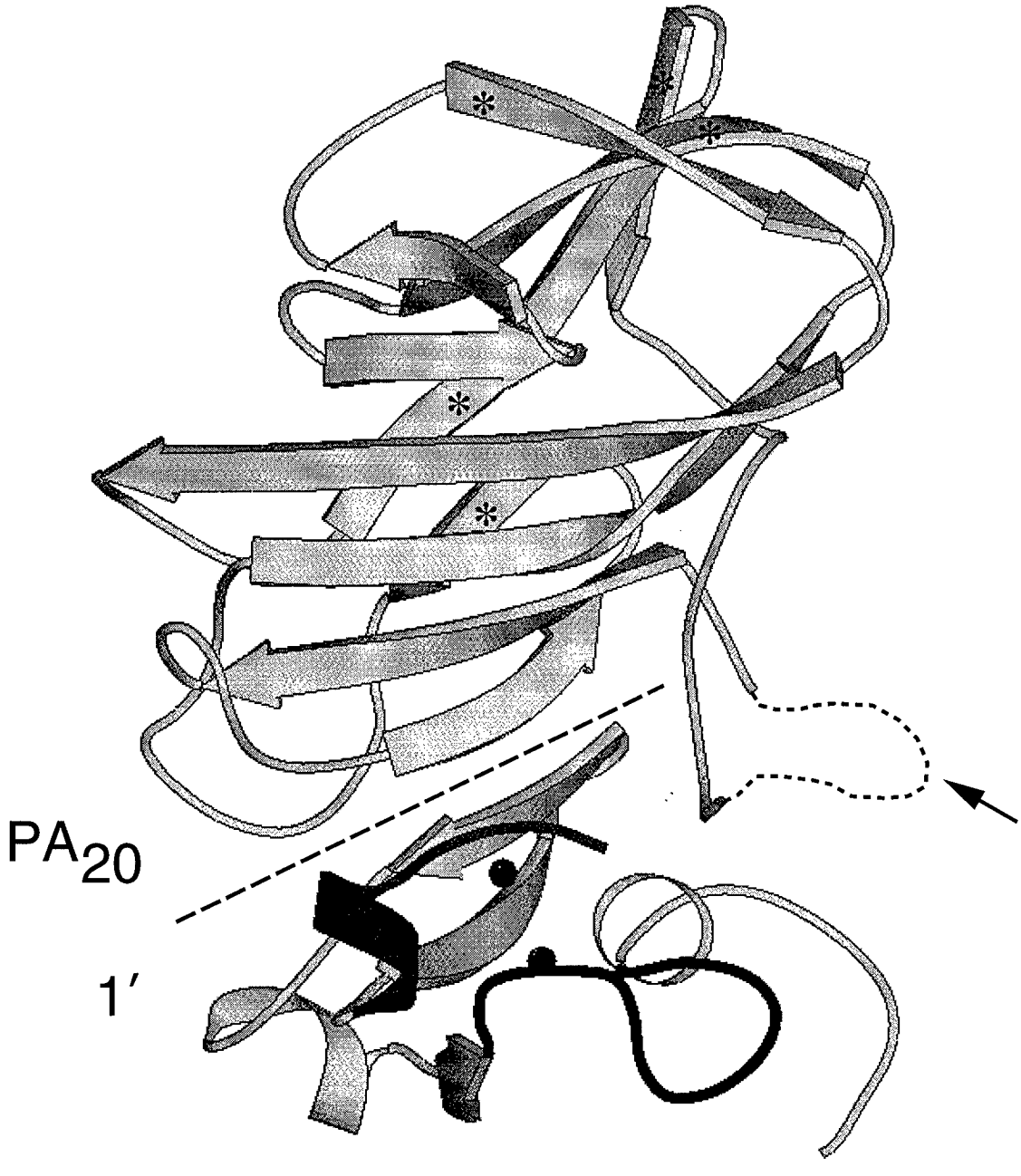


**Fig. 4.** Domain 1. The large β sheet is in the foreground and the small one, marked with asterisks, is in the background. Calcium–binding loops are highlighted and the two calcium ions are shown in black. The arrow indicates the furin cleavage site located in a disordered loop (dotted line). The dashed line separates PA20 from domain 1'.

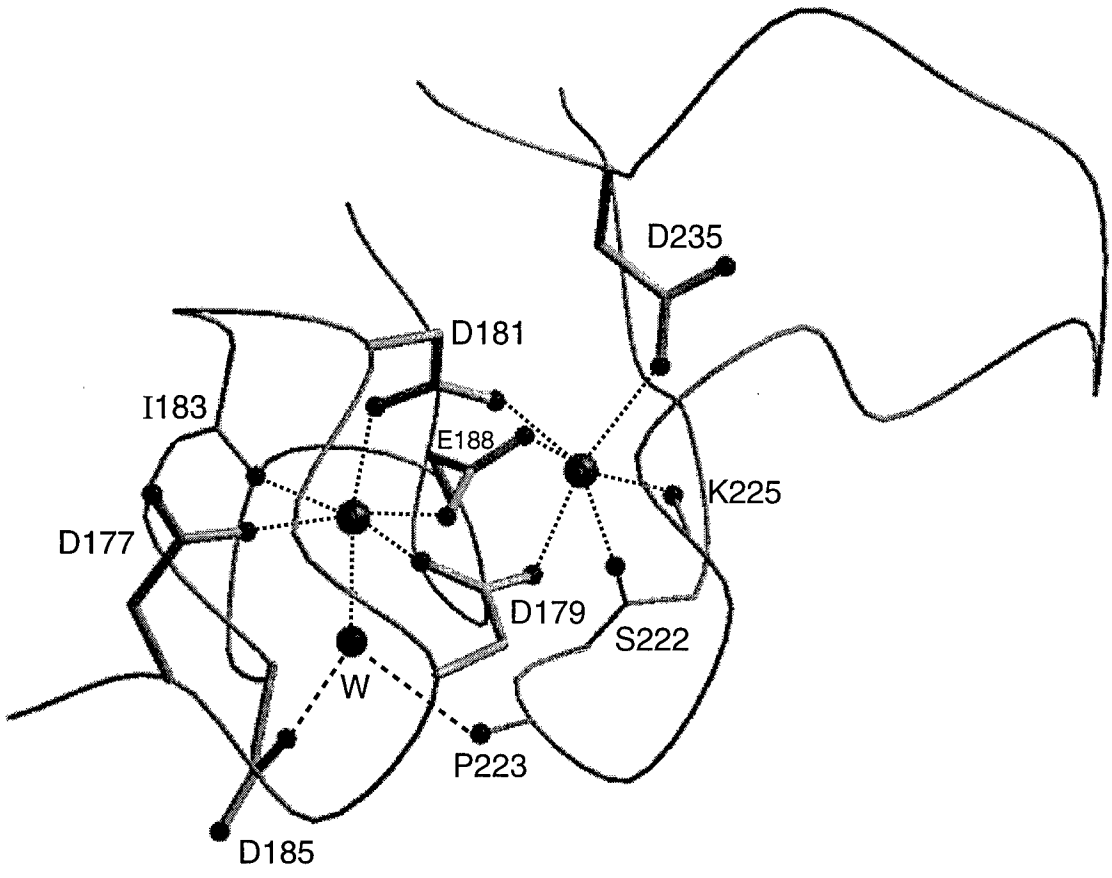


**Fig. 5.** The calcium binding site. The calcium ions are shown as large spheres. Ca1 (left) is coordinated by the carboxylate oxygens of D177, D179, and E188, the carbonyl oxygen of I183 and by a water molecule (W), which in turn is hydrogen bonded to a carboxylate oxygen of D185 and to the carbonyl oxygen of P223. The calcium binding loop formed by residues 177–188 conforms to the canoncial EF–hand. Ca2 (right) is coordinated by carboxylate oxygens of D179, D181, E188 and D235, and the carbonyl oxygens of S222 and K225.

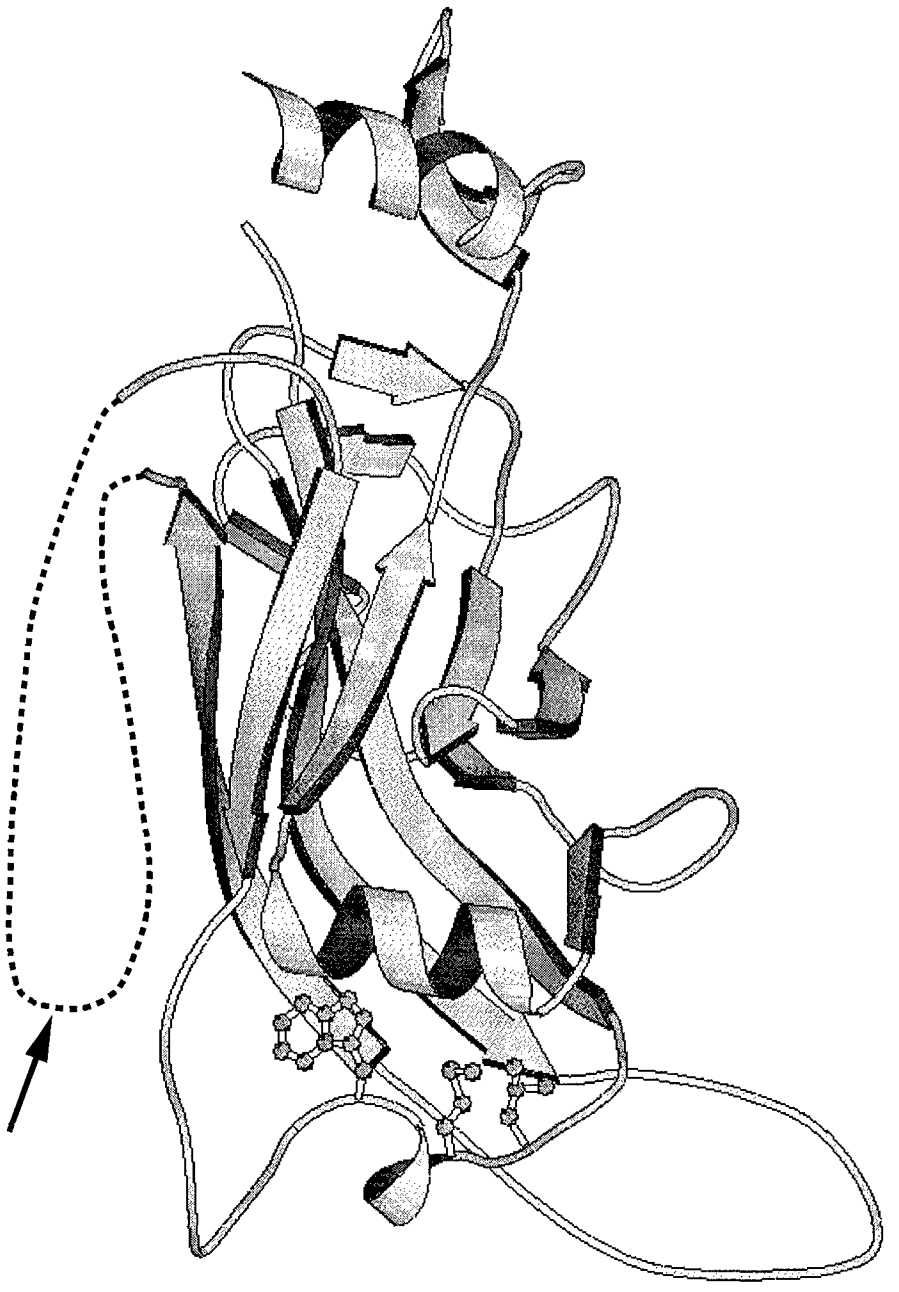

**Fig. 6.** Domain 2. The arrow indicates the chymotrypsin cleavage site in the large loop implicated in membrane insertion. Residues Trp346, Met350 and Leu352 of loop 3 are shown in the buried conformation they adopt in crystal form 1 (pH 7.5); they are disordered in crystal form 2 (pH 6.0).

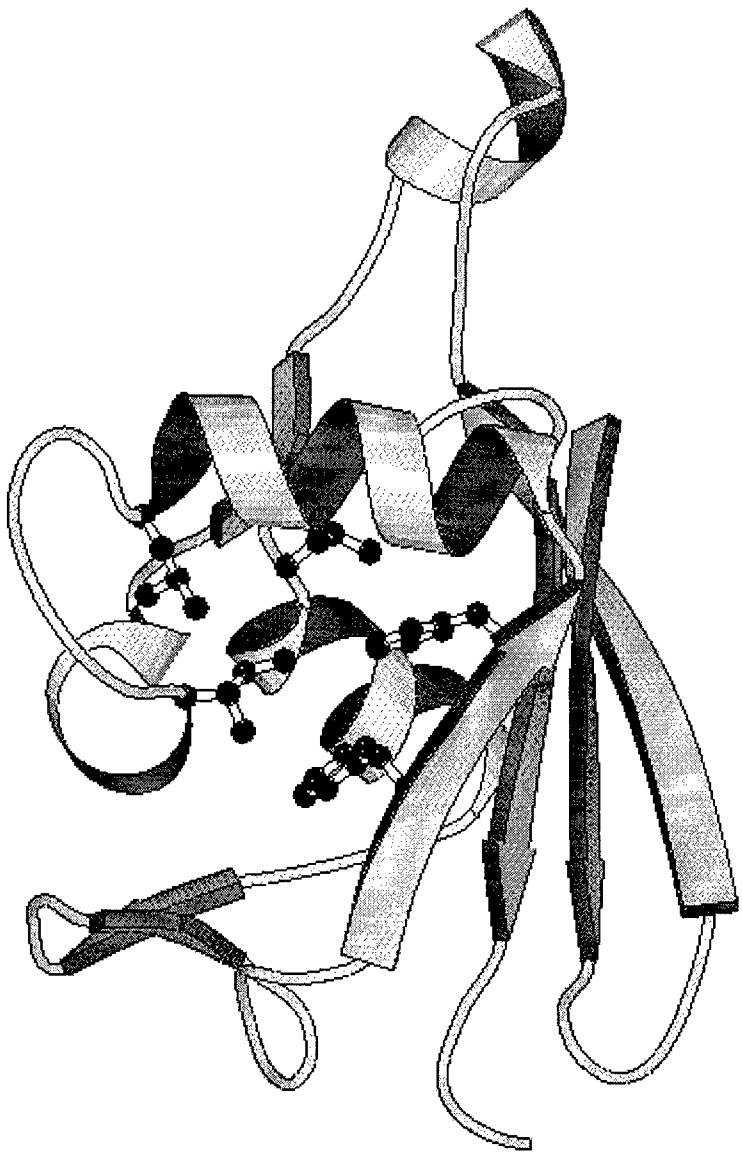

**Fig. 7.** Domain 3. The residues forming the hydrophobic patch (Phe552, Phe554, Ile562, Leu 566 and Ile574) are shown. In crystals of PA this patch is occupied by a Phe from a neighboring molecule (not shown).

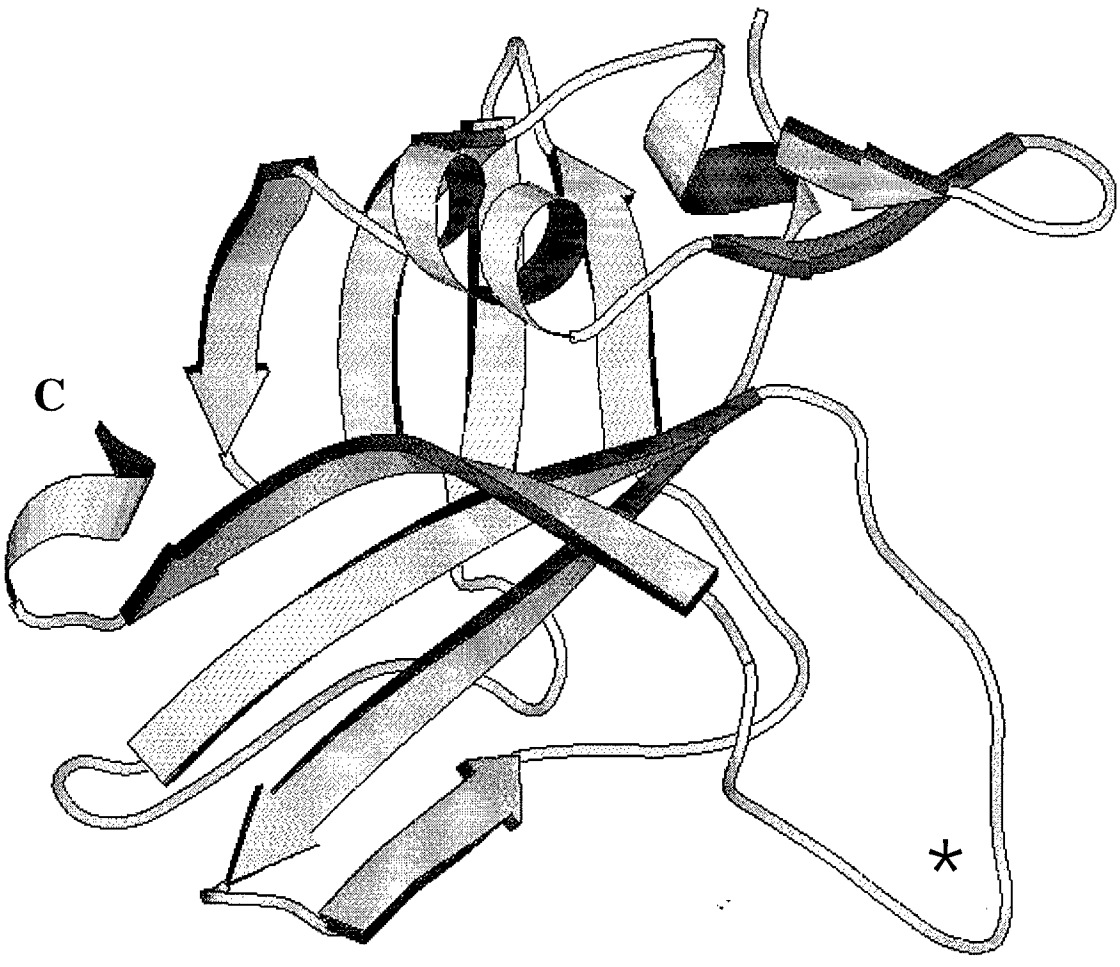


**Fig. 8.** Domain 4. The C–terminus is indicated. The β hairpin which packs against domain 3 is at the top right and the large loop which is likely important for receptor binding activity is marked by an asterisk.


**Fig. 9.** The model of the PA63 heptamer, viewed down the heptamer axis, with domain 1' nearest the viewer and domain 4 the furthest.

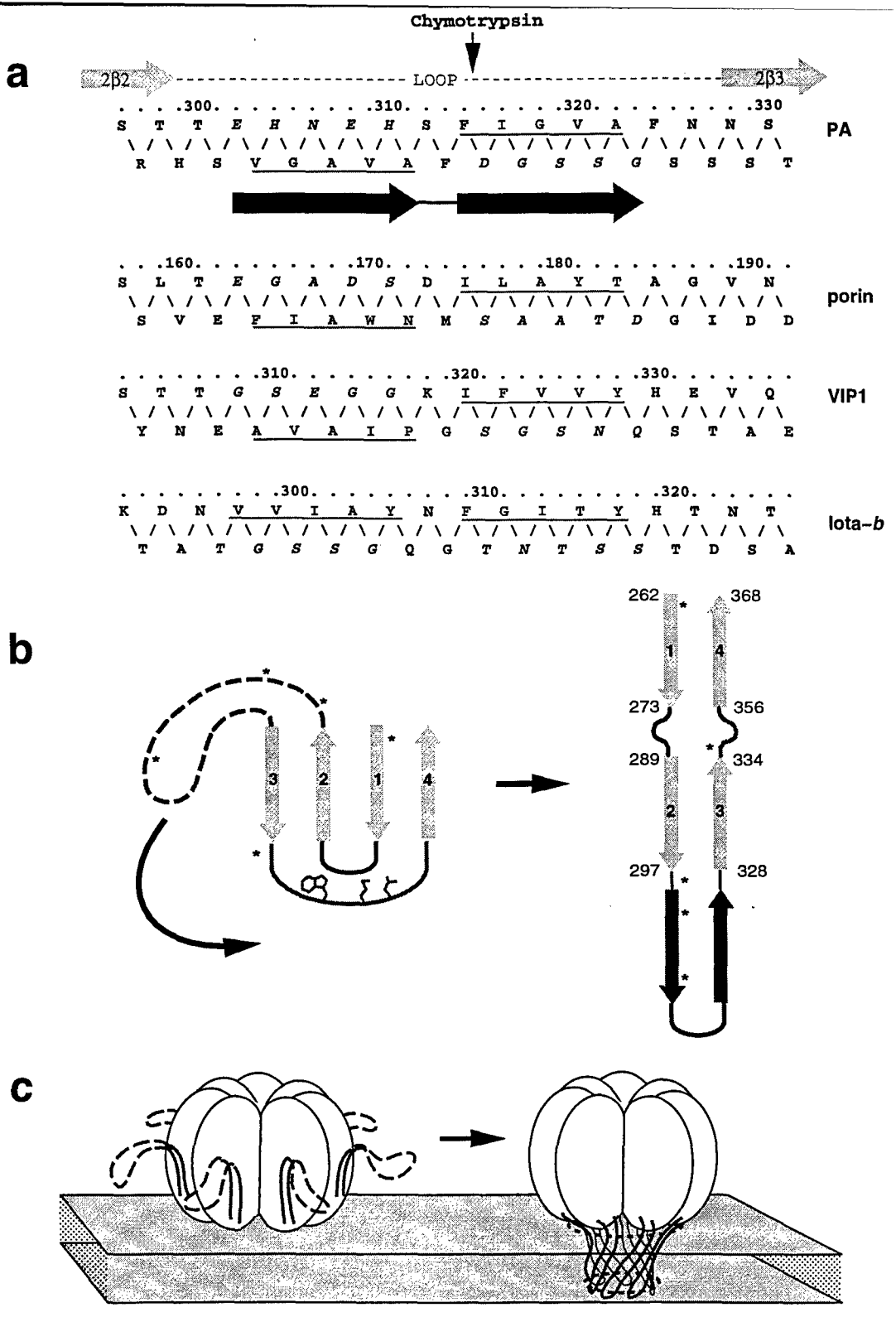


**Fig. 10.** Proposed mechanism of membrane insertion. (**a**) Amphipathic hairpin formation by the chymotrypsin-sensitive loop. Residues 302–311 form one strand of the hairpin and 314–324 form the other. Residues forming the hydrophobic face are underlined. The sequences of iota–*b*, VIP1 and αHLare also shown for comparison. (**b**) Unfolding of the Greek key motif formed by strands 1–4 of domain 2. Hisitidine positions are shown as asterisks. (**c**) Association of the seven β–hairpins in the $PA_{63}$ heptamer to form a 14–stranded membrane–inserted β barrel.

## *REFERENCES*


1. R. Koch, *Beitr. Biol. Pflanz.* **2**, 277 (1877). The aetiology of anthrax based on the ontogeny of the anthrax bacillus.

2. W. S. Greenfield, *Proc. R. Soc. (London)* **30**, 557 (1880).

3. L. Pasteur, *Comptes rendus hebdomadaires des séances de l'Académie des Sciences.* **92**, 429 (1881). De l'attenuation des virus et de leur retour a la virulence.

4. T. Fujikura, in *Proceedings of the international workshop on anthrax* P. C. B. Turnbull, Ed. (Salisbury Medical Society, Winchester, England, 1989), vol. 68, pp. 1.

5. N. Zenova, "The deadly cloud over Sverdlovsk," *Wall Street Journal* 1990, pp. Nov. 28 p.A22.

6. P. Gumbel, "The anthrax mystery./Death in the air/The survivors speak.," *Wall Street Journal* 1991, pp. Oct. 21, p.A18; Oct 22, p.A20; Oct 23, p. A14.

7. M. Meselson, et al., *Science* **266**, 1202-8 (1994). The Sverdlovsk anthrax outbreak of1979.

8. R. J. Manchee, M. G. Broster, *Nature* **294**, 254 (1981).

9. P. Turnbull, in *Topley and Wilson's Principles of Bacteriology, Virology and Immunity: Bacterial Diseases.* G. R. Smith, C. S. F. Easman, Eds. (Edward Arnold, London, 1990), vol. 3, pp. 365-79.

10. P. S. Brachman, in *Bacterial infections of humans: epidemiology and control* A. S. Evans, P. S. Brachman, Eds. (Plenum, New York, 1991) pp. 75-86.

11. S. H. Leppla, in *Sourcebook of Bacterial Protein Toxins* J. E. Alouf, J. H. Freer, Eds. (Academic Press, San Diego, 1991) pp. 277-302.

12. S. H. Leppla, in *Bacterial Toxins and Virulence Factors in Disease.* J. Moss, B. Iglewksi, M. Vaughan, A. T. Tu, Eds. (Marcel Dekker, New York, 1995) pp. 543-72.

13. J. L. Stanley, J. Sargeant, H.Smith, *J. Gen. Microbiol.* **22**, 206-18 (1960).

14. A. M. Friedlander, *J. Biol. Chem.* **261**, 7123-26 (1986). Macrophages are sensitive to anthrax lethal toxin through an acid-dependent process.

15. J. W. Ezzell, B. E. Ivins, S. H. Leppla, *Infect. Immun.* **45**, 761-7 (1984). Immunoelectrophoretic analysis, toxicity and kinetics of in vitro production of the protective antigen and lethal factor components of *Bacillus anthracis* toxin.

16. V. Escuyer, R. J. Collier, *Infect. Immun.* **59**, 3381-86 (1991). Anthrax protective antigen interacts with a specific receptor on the surface of CHO-K1 cells.

17. K. R. Klimpel, S. S. Molloy, G. Thomas, S. H. Leppla, *Proc. Natl. Acad. Sci. U.S.A.* **89**, 10277-81 (1992). Anthrax toxin protective antigen is activated by a cell surface protease with the sequence specificity and catalytic properties of furin.

18. V. M. Gordon, K. R. Klimpel, N.Arora, M.A.Henderson, S.H.Leppla, *Infect. Immun.* **63**, 82-87 (1995). Proteolytic activation of bacterial toxins by eukaryotic cells is performed by furin and by additional cellular proteases.

19. J. C. Milne, D. Furlong, P. C. Hanna, J. S. Wall, R. J. Collier, *J. Biol. Chem.* **269**, 20607-12 (1994). Anthrax protective antigen forms oligomers during intoxication of mammalian cells.

20. R. O. Blaustein, T. M. Koehler, R. J. Collier, A. Finkelstein, *Proc. Natl. Acad. Sci. USA* **86**, 2290-13 (1989). Anthrax toxin: channel-forming activity of protective antigen in planar phospholipid bilayers.

21. J. C. Milne, R. J. Collier, *Mol. Microbiol.* **10**, 647-53 (1993). pH-dependent permeabilization of the plasma membrane of mammalian cells by anthrax protective antigen.

22. V. M. Gordon, S. H. Leppla, E. L. Hewlett, *Infect. Immun.* **56**, 1066-69 (1988). Inhibitors of receptor-mediated endocytosis block the entry of *Bacillus anthracis* adenylate cyclase toxin but not that of *Bordetella pertussis* adenylate cyclase toxin.

23. S. H. Leppla, *Proc. Natl. Acad. Sci. U.S.A.* **79**, 3162-66 (1982). Anthrax toxin edema factor: a bacterial adenylate cyclase that increases cyclic AMP concentrations in eukaryotic cells.

24. S. H. Leppla, *Adv. Cyclic Nucleotide Protein Phosphorylation Res.* **17**, 189-98 (1984). *Bacillus anthracis* calmodulin-dependent adenylate cyclase: chemical and enzymatic properties and interactions with eukaryotic cells.

25. G. M. Gill, in *Bacterial toxins and cell membranes* J. Jeljaszewicz, T. Wadstrom, Eds. (Academic Press, New York, 1978) pp. 291-314.

26. S. Perelle, M. Gibert, P. Boquet, M. R. Popoff, *Infect. Immun.* **61**, 5147-56 (1993). Characterization of *Clostridium perfringens* Iota-Toxin genes and expression in *Escherichia coli.*

27. G. Warren, et al. *World intellectual property organization* (U.S., 1996) pp. 235. Novel pesticidal proteins and strains. Patent application No.: WO 96/10083

28. J. L. Stanley, H. Smith, *J. Gen. Microbiol.* **31**, 329-37 (1963). The three factors of anthrax toxin: their immunogenicity and lack of demonstrable enzymic activity.

29. P. Hambleton, J. A. Carman, J. Melling, *Vaccine* **2**, 125-132 (1984). Anthrax: the disease in relation to vaccines.

30. P. C. Turnbull, *Vaccine* **9**, 533-39 (1991). Anthrax vaccines: past, present, and future.

31. B. E. Ivins, S. K. Welkos, S. F. Little, G. B. Knudson, in *Proceedings of the international workshop on anthrax.* P. C. B. Turnbull, Ed. (Salisbury Medical Society, Winchester, England, 1989), vol. 68, pp. 86-88.

32. P. C. B. Turnbull, M. G. Broster, J. A. Carman, R. J. Manchee, J. Melling, *Infect Immun* **52**, 356-63 (1986). Development of antibodies to protective antigen and

lethal factor components of anthrax toxin in humans and guinea pigs and their relevance to protective immunity.

33. S. F. Little, G. B. Knudson, *Infect Immun* **52**, 509-12. (1986). Comparative efficacy of *Bacillus anthracis* live spore vaccine and protective antigen vaccine against anthrax in the guinea pig.

34. I. Pastan, V. Chaudhary, D. J. Fitzgerald, *Ann. Rev. Biochem.* **61**, 331-54 (1992). Recombinant toxins as novel therapeutic agents.

35. C. Petosa, R. J. Collier, K. R. Klimpel, S. H. Leppla, R. C. Liddington, *Nature* In press. (1997). Crystal structure of the anthrax toxin protective antigen.

36. Z. Otwinowski, in *Data collection and processing* L. Sawyer, N. Isaacs, S. Bailey, Eds. (Science and Engineering Research Council, Warrington, United Kingdom, 1993) pp. 56-62.

37. A. J. Howard, et al., *Methods Enzymol.* **114**, 452 (1985). (UCSD software).

38. Z. Otwinowski, in *Proceedings of the CCP4 Study Weekend: Isomorphous Replacement and Anomalous Scattering* . (Daresbury Laboratory, 1991) pp. 80-85.

39. T. A. Jones, *J. Appl. Cryst.* **11**, 268-72 (1978). A graphics model building and refinement system for macromolecules.

40. A. T. Brünger, *X-PLOR Manual version 3.1.* Y. University, Ed. (New Haven, CT, 1992).

41. G. Kleywegt, T. A. Jones, in *From first map to final model* S. Bailey, R. Hubbard, D. Waller, Eds. (SERC Daresbury Laboratory, Warrington, U.K., 1994) pp. 59-66.

42. S. F. Little, et al., *Microbiology-UK* **142**, 707-715 (1996). Characterization of lethal factor-binding and cell-receptor binding domains of protective antigen of *Bacillus anthracis* using monoclonal antibodies.

43. J. M. Novak, M.-P. Stein, S. F. Little, S. H. Leppla, A. M. Friedlander, *J. Biol. Chem.* **267**, 17186-93 (1992). Functional characterization of protease-treated *Bacillus anthracis* protective antigen.

44. Y. Singh, K. R. Klimpel, C. P. Quinn, Y. K. Chaudhary, *J. Biol. Chem.* **266**, 15493-97 (1991). The carboxyl-terminal end of protective antigen is required for receptor binding and anthrax toxin activity.

45. S. Choe, et al., *Nature* **357**, 216-22 (1992). The crystal structure of diphtheria toxin.

46. J. Zhao, J. C. Milne, R. J. Collier, *J. Biol. Chem.* **270**, 18626-30 (1995). Effect of anthrax toxin's lethal factor on ion channels formed by the protective antigen.

47. Y. Singh, K. R. Klimpel, N. Arora, M. Sharma, S. H. Leppla, *J. Biol. Chem.* **269**, 29039-46 (1994). The chymotrypsin-sensitive site, $FFD^{315}$, in anthrax toxin protective antigen is required for translocation of lethal factor.

48. L. Song, et al., *Science* **274**, 1859-65 (1996). Structure of Staphylococcal α-hemolysin, a heptameric transmembrane pore.

49. R. O. Blaustein, A. Finkelstein, *J. Gen. Physiol.* **96**, 905-19 (1990). Voltage-dependent block of anthrax toxin channels in planar phospholipid bilayer membranes by symmetric tetraalkylammonium ions.

50. J. W. Kelly, *Curr. Op. Struct. Biol.* **6**, 11-17 (1996). Alternative conformations of amyloidogenic proteins govern their behavior.

51. T. M. Koehler, R. J. Collier, *Mol. Microbiol.* **5**, 1501-6 (1991). Anthrax toxin protective antigen: low pH-induced hydrophobicity and channel formation in liposomes.

52. N. Arora, S. H. Leppla, *J.Biol.Chem.* **268**, 3334-41 (1993). Residues 1-254 of anthrax toxin lethal factor are sufficient to cause cellular uptake of fused polypeptides.

53. S. R. Blanke, J. C. Milne, E. L. Benson, R. J. Collier, *Proc.Natl.Acad.Sci.USA* **93**, 8437-8442 (1996). Fused polycationic peptide mediates delivery of diphtheria toxin A chain to the cytosol in the presence of anthrax protective antigen.

## *BIBLIOGRAPHY*

*Personnel receiving pay:* Robert Liddington, Ph.D., Carlo Petosa, Ph.D., João Cabral, Ph.D., Jadwiga Bienkowska, Ph.D., Christin Frederick, Ph.D., Lorraine Mulry, Florence Poy

*Publications:*

Petosa C and Liddington RC. The anthrax toxin. In: *Protein Toxin Structure.* M. W. Parker, ed. R.G.Landes Biomedical, Austin, Texas. pp. 97-121. 1996.

Petosa C, Collier RJ, Klimpel K, Leppla SH and Liddington RC. Crystal structure of the anthrax toxin protective antigen. *Nature* In press, 1997.

*Meetings:*

C. Petosa and R.C. Liddington. Structure of the anthrax protective antigen. Annual meeting of the American Crystallographic Association, Montreal, July 1995. Vol. 23. p.61. Abstract ref. 2a.6.A.

C. Petosa and R.C. Liddington. Crystal structure of the anthrax protective antigen. Fifth international conference on Biophysics and Synchrotron Radiation, Grenoble, France, August 1995. Session 11. Abstract reference 01-25.

C. Petosa (Oral presentation). Crystal structure of anthrax protective antigen. Gordon Research Conference on Microbial Toxins and Pathogenesis, Proctor Academy, Andover, N.H. July 1996.

C. Petosa (Oral presentation). Structure of the Anthrax Toxin Protective Antigen. Workshop on Pore-forming toxins. Mainz, Germany. September, 1996.